PHYSICAL REVIEW A VOLUME 28, NUMBER 1 JULY 1983

Spontaneous radiation from relativistic electrons in a tapered undulator

P. Bosco and W. B. Colson
Department of Physics and Quantum Institute, University of California, Santa Barbara, California 93106
(Received 20 January 1983)

The spectrum, angular distribution, polarization, and coherence properties of the radiation emitted by relativistic electrons undulating through a quasiperiodic tapered magnetic field are studied. Tapering the wavelength and/or field strength along the undulator's axis has the effect of spreading the spectral line to higher frequencies; interference over this broader spectral range results in a more complex line shape. The angular dependence, on the other hand, is not affected by the amount of taper. The polarization of the radiation in the forward direction is determined by the transverse polarization of the undulator, but the polarization changes off axis. The radiation patterns predicted here are distinct from those of untapered undulators and their detection is now feasible. They will provide useful diagnostics of electron trajectories and threshold behavior in free-electron-laser oscillators using tapered undulators.

INTRODUCTION

Charged particles traveling along the axis of a static, undulating magnetic field execute transverse oscillations. The resulting acceleration radiation from relativistic electrons ("magnetic bremsstrahlung"[1–7]) is emitted into a narrow cone in the forward direction. The Doppler shifted spectrum is peaked at a much higher frequency than the electron oscillation frequency. The polarization of the radiation in the forward direction is determined by the configuration of the undulating magnetic field and resulting particle motion; a helical array of magnets produces circularly polarized light while a linear array produces linearly polarized light. As the detector is moved off axis the emission spectrum shifts down in frequency, decreases, and the polarization changes.[4–7] A trajectory with many small transverse excursions produces a spectrum with a few narrow peaks at the low-order harmonics. The magnetic field generating this type of radiation is called an "undulator," while the term "wiggler" is reserved for magnetic fields with only a few periods and larger excursions which generate broadband synchrotron radiation.[4,5]

In a free electron laser (FEL),[8,9] the magnetic bremsstrahlung is stored in an optical resonator to provide feedback for subsequent stimulated magnetic bremsstrahlung. The optical gain at various frequencies, angles, and harmonics depends on the undulator design and the resulting electron trajectories through the undulator. The evolution from spontaneous to stimulated emission also depends on that design. These important characteristics are known for the simple periodic undulator, but less is known about the tapered undulator which represents an important modification for high-power FEL operation.[10–12] In a tapered undulator the magnet's wavelength and/or field strength are varied along its length to preserve the same Doppler shift while the electrons lose energy to the optical field. This improves the energy extraction efficiency from the electrons when operating at high optical power levels. A physical picture of this process can be given in terms of electron trapping and deceleration in the potential "bucket" generated by the combined action of the laser and the static fields.[11,12]

However, the same tapered undulator design that improves energy extraction efficiency in strong optical fields reduces the electron-optical coupling in weak fields. This is caused by the broader spectral range of the tapered undulator, and the details of the reduced coupling can be investigated directly from the spontaneous emission spectrum. Furthermore, in any real experimental situation one must include a study of the spectrum off axis since resonator modes extend over a finite range of angles. Detailed knowledge of the emission spectrum can be a useful diagnostic tool in determining the paths of electrons through the undulator. The forward emission spectrum in the fundamental line from a linearly tapered undulator has been calculated analytically.[13] We present the spectrum's full angular distribution in higher harmonics for a wide range of tapers. The polarization of the emitted radiation is also examined. For helical undulators we show that the polar-

ization changes from circular to linear at a well-defined angle, regardless of the tapering. Because of its analytical simplicity the focus is mainly on the helical undulator design, but some results are presented for the linearly polarized field design to highlight their differences.

I. ELECTRON TRAJECTORIES

The spontaneous emission spectrum is determined by the electron trajectories in the undulator. Neglecting radiation losses ($\dot{\gamma}=0$), the equation of motion for an electron in a magnetic field is

$$\frac{d\vec{\beta}}{dt}=-\frac{e}{\gamma mc}(\vec{\beta}\times\vec{\mathrm{B}}) \ , \tag{1.1}$$

where $e=|e|$ is the electron charge, m is the electron mass, $c\vec{\beta}$ is the electron velocity, γmc^2 is the electron energy, and c is the speed of light.

A circularly polarized magnetic field inside the undulator has the form

$$\vec{\mathrm{B}}=B(z)(\cos\Psi(z),\sin\Psi(z),0) \ , \tag{1.2}$$

where

$$\Psi(z)=\int_0^z dz' k_0(z')=[1+\eta z/2L(\eta)]k_0 z \ ,$$

$\lambda_0(z)=2\pi/k_0(z)$ is the undulator's wavelength at z, and $\lambda_0=2\pi/k_0$ is the undulator's wavelength at $z=0$. The parameter η describes a linear taper of the undulator's wave vector. The length of the undulator $L(\eta)$ is a function of taper η and is the sum of all tapered wavelengths. This gives

$$\begin{aligned}L&=\lambda_0\sum_{i=1}^{N}\left[1+\eta\left[\frac{i-1}{N-1}\right]\right]^{-1}\\&=\lambda_0\left[N-\frac{\eta}{N-1}\left[\frac{N(N-1)}{2}\right]+\frac{\eta^2}{(N-1)^2}\left[\frac{N(N-1)(2N-1)}{6}\right]-\cdots\right]\\&=N\lambda_0\left[1-\frac{\eta}{2}+\frac{\eta^2}{6}\left[\frac{2N-1}{N-1}\right]-\frac{\eta^3}{4}\left[\frac{N}{N-1}\right]+\cdots\right] \ ,\end{aligned} \tag{1.3}$$

where N is the number of undulator periods. For long undulators ($N\gg1$)

$$L(\eta)\approx N\lambda_0\sum_{k=0}^{\infty}\frac{(-\eta)^k}{k+1}=L_0\frac{\ln(1+\eta)}{\eta} \ , \tag{1.4}$$

where $L_0=L(0)=N\lambda_0$ is the undulator length with no taper.

We consider the particular case in which the amplitude of the magnetic field is also a linear function of z such that

$$B(z)=B_0[1+\eta z/L(\eta)]$$

and the dimensionless ratio $K=eB(z)/k_0(z)mc^2$ is constant throughout the undulator. Typical values of K for an undulator are of order unity. (If $K\gg1$ the array of magnets becomes a broadband wiggler.[4,5]) Both $k_0(z)$ and $B(z)$ can be used to "tune" the Doppler shift along the undulator's length, but the special case where K is constant is analytically simpler. The Stanford undulator, although untapered, gives typical values of $\lambda_0=3.2$ cm and $B_0=2.4$ kG, and uses a 40-MeV electron beam ($\gamma=80$) so that $K=0.7$. A typical tapered undulator has $L\approx160$ cm and $\eta\approx0.05$ with fields and wavelengths similar to the Stanford untapered case.

The transverse equations can be integrated immediately because K is constant:

$$\begin{aligned}\beta_x(t)&=\frac{K}{\gamma}(1-\cos\Psi)+\beta_x(0) \ ,\\ \beta_y(t)&=-\frac{K}{\gamma}\sin\Psi+\beta_y(0) \ ,\end{aligned} \tag{1.5a}$$

$$\beta_z=\left[1-\frac{(1+K^2)}{\gamma^2}\right]^{1/2}=\beta_0=\text{const.} \tag{1.5b}$$

The constants of integration $\beta_x(0)$ and $\beta_y(0)$ can be chosen to insure that the beam does not drift in the transverse directions. This requirement gives the conditions for "perfect injection":

$$\beta_x(0)=-\frac{K}{\gamma}, \ \beta_y(0)=0 \ . \tag{1.5c}$$

Integrating (1.5b) gives $z(t)=c\beta_0 t+z(0)$. The transverse oscillations are obtained by direct integration of (1.5a) using $z(t)$ in $\Psi(z)$:

$$x(t)=-\frac{K\lambda_0 s}{\gamma\beta_0}\{\cos(2\pi s^2)[C(q)-C[(2s)] +\sin(2\pi s^2)[S(q)-S(2s)]\}+x(0) \ ,$$
$$y(t)=-\frac{K\lambda_0 s}{\gamma\beta_0}\{\cos(2\pi s^2)[S(q)-S(2s)] -\sin(2\pi s^2)[C(q)-C(2s)]\}+(2s)]\}+y(0) \ , \tag{1.6}$$

where $s^2=L(\eta)/2\eta\lambda_0$,

$$q=2s[1+\eta c\beta_0 t/L(\eta)] \ ,$$

$S(q)$ and $C(q)$ are Fresnel integrals and $z(0)=0$ for simplicity. For undulators with a number of periods $N\gg 1$ with the $\eta\leq 1$ the arguments of the Fresnel integrals are large. Using their asymptotic expansions[14] and keeping only the leading term in q^{-1} we obtain

$$x(\tau)=-\frac{K\lambda_0}{2\pi\gamma}\left[\frac{\sin\Psi(\tau)}{1+\eta\tau}\right]+x(0) \ ,$$
$$y(\tau)=-\frac{K\lambda_0}{2\pi\gamma}\left[1-\left[\frac{\cos\Psi(\tau)}{1+\eta\tau}\right]\right]+y(0) \ , \tag{1.7}$$

where

$$\Psi(\tau)=k_0 L(\eta)\tau(1+\eta\tau/2) \ ,$$

and $\tau=c\beta_0 t/L(\eta)$ so that $0\leq\tau\leq 1$ for any trajectory. Both results (1.6) and (1.7) are new and relevant to the explicit angular dependence of the spectrum that will be calculated in Sec. IV.

The function $x(\tau)$ is plotted in Fig. 1 for the values $\eta=1.0$, $x_0(0)=0$, and $N=10$ periods in the undulator. A similar plot would describe $y(\tau)$. Both the wavelength and the amplitude of the oscillations decrease while keeping K constant. A typical amplitude of the transverse oscillations is $K\lambda_0/2\pi\gamma\approx 10^{-2}$ cm. There is an upper limit on $K/\gamma\leq 0.369$ for stable orbits in untapered undulators.[15]

To insure that all the electrons in a beam follow helical orbits along the same axis of the undulator, we must choose the initial position $x(0)$ and $y(0)$ so that

$$\int_0^1 x(\tau)d\tau=\int_0^1 y(\tau)d\tau=0 \ ,$$

The integration can be performed numerically to find that for values of η less than unity

$$|x(0)|\leq 0.057K\lambda_0/2\pi\gamma \ , \quad |y(0)|\leq 0.998K\lambda_0/2\pi\gamma.$$

Since typical electron beams have a $d\approx 1$ mm diameter this condition cannot be met for all electrons. Most electrons travel in parallel but identical helices. The characteristic emission angle for relativistic electrons is γ^{-1} so that the light emitted with wavelength λ adds coherently from all electrons within a beam of diameter d if $d\leq\gamma\lambda$. This condition is not met for typical experiments since $\gamma\lambda\approx 0.2$ mm, and coherent emission is only possible over a narrow range of emission angles. Fortunately, in an FEL, the high-Q resonator selects a much narrower range of angles naturally so that all electrons participate coherently.

II. TOTAL ENERGY RADIATED

We can use the formula of Liénard[16] to express the total electromagnetic energy radiated:

$$E_{\rm tot}=\int_{-\infty}^{\infty}\frac{2e^2\gamma^6}{3c}\left[\left[\frac{d\vec{\beta}}{dt}\right]^2-\left[\vec{\beta}\times\frac{d\vec{\beta}}{dt}\right]^2\right]dt \ . \tag{2.1}$$

Using (1.5) we obtain

$$E_{\rm tot}=\tfrac{2}{3}e^2\gamma^2K^2k_0^2\beta_0 L(\eta)(1+\eta+\eta^2/3) \ . \tag{2.2}$$

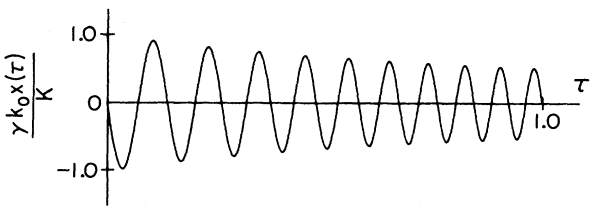

FIG. 1. Electron trajectories in a tapered undulator. Electron is shown to "undulate" in phase with the magnetic field. Amplitude and wavelength of the oscillations decrease to keep $K=eB(z)/k_0(z)mc^2$ constant along z.

For small amounts of tapering, and using (1.4),

$$E_{\rm tot}\approx\tfrac{2}{3}\,e^2\gamma^2K^2k_0^2\beta_0L_0\left[1+\frac{\eta}{2}+\frac{\eta^2}{6}+\cdots\right]\ . \tag{2.3}$$

Notice that $E_{\rm tot}$ increases in proportion to γ^2K^2 and increases with η because the electron is forced into a tighter spiraling motion. Typical numerical values ($\gamma\approx80$, $K\approx0.7$, $L_0\approx1.6$ m, $\lambda_0\approx3$ cm) give $E_{\rm tot}\approx0.1$ eV. This justifies neglecting radiation losses in Sec. I since $E_{\rm tot}\ll\gamma mc^2$.

III. LIÉNARD-WIECHERT FIELDS

The radiation fields from accelerating electrons can also be investigated by using the Liénard-Wiechert fields.[16] The electric field at the observation position $\vec{D}=D\hat{n}=D(\sin\vartheta\cos\varphi,\ \sin\vartheta\sin\varphi,\ \cos\vartheta)$ created by an electron at $\vec{r}(t)$ is

$$\vec{E}(\vec{D},t)=-\left[\frac{e}{\kappa^3}\left[\frac{(\hat{n}-\vec{\beta})}{\gamma^2R^2}+\frac{\hat{n}\times[(\hat{n}-\vec{\beta})\times(d\vec{\beta}/dt)]}{cR}\right]\right]_{\rm ret}\ , \tag{3.1}$$

where $\vec{R}(t')=\vec{D}-\vec{r}(t')$ and $\kappa=1-\hat{n}\cdot\vec{\beta}(t')$. The quantity in large parentheses is evaluated at the retarded time given by $t'=t-R(t')/c$. In the far field limit (R large) and in the forward direction ($\vartheta=0$), $R(t')\approx(D-c\beta_0t')$. Using (1.7) and $\Psi(\tau)$ defined there we get

$$\vec{E}(t)\,|_{\vartheta=0}\approx\frac{4\gamma^3eKk_0(1+\eta\tau')}{(1+K^2)^2[D-\tau'L(\eta)]}\times(\sin\Psi(\tau'),-\cos\Psi(\tau'),0)\ , \tag{3.2}$$

where

$$\tau'=\frac{2\gamma^2(ct-D)}{(1+K^2)L(\eta)}\ \text{and}\ \gamma\gg1\ .$$

The radiation is substantially Doppler shifted to higher frequencies for relativistic electrons due to the γ^2 factor in Ψ. This feature gives the FEL its wide tunable range to short wavelengths. For typical parameters the emitted wavelength is $\sim3\mu$. The effect of tapering is to introduce more Fourier components into the oscillation spectrum, thus complicating the line shape. The forward radiation is circularly polarized because of the helical undulator design.

It is interesting to investigate whether quantum effects might play a role in the emission process. The number of photons emitted by a single electron per pass through the undulator is approximately $E_{\rm tot}/\hbar\omega$ ignoring emission into higher harmonics ($K\leq1$) and the taper ($\eta\ll1$). The photon frequency from (3.2) is $\omega\approx2\gamma^2\omega_0$, where $\omega_0=ck_0$. Then, using (2.3), $E_{\rm tot}/\hbar\omega\leq1$. The classical results must therefore be interpreted as representing the average energy emitted and the photon statistics left to another calculation.

Now consider the emission from a beam of N_e electrons. Interference effects due to the phase differences introduced by the initial position $\vec{r}_j(0)$ of the jth electron have to be taken into consideration. The effects of the transverse distribution of initial positions has been discussed. The effects of the longitudinal distribution of initial electron phases

$$\zeta_j=2\gamma^2k_0z_j(0)/(1+K^2)$$

is found by summing the contributions from all the electrons using (3.2):

$$\vec{E}_{\rm tot}(t)=\sum_{j=1}^{N_e}\vec{E}_j(t)=\sum_{j=1}^{N_e}\frac{4\gamma^3eKk_0(1+\eta\tau')}{(1+K^2)^2[D-\tau'L(\eta)]}(\sin[\Psi(\tau')+\zeta_j],-\cos[\Psi(\tau')+\zeta_j],0)$$

$$=\frac{4\gamma^3eKk_0(1+\eta\tau')A}{(1+K^2)^2[D-\tau'L(\eta)]}(\sin[\Psi(\tau')+Z],-\cos[\Psi(\tau')+Z],0)\ , \tag{3.3}$$

where

$$A^2=N_e+2\sum_{i>j}^{N_e}\cos(\zeta_i-\zeta_j)\ ,$$

$$Z=\tan^{-1}\left[\frac{\langle\sin\zeta_j\rangle}{\langle\cos\zeta_j\rangle}\right]\ ,$$

and the angular brackets indicate an average over all N_e electrons (i.e., $N_e^{-1}\sum_{j=1}^{N_e}$). When $N_e\gg1$ and the phases are completely random $A\approx\sqrt{N_e}$. The radiated power detected will then be proportional to N_e and during the initial stages of start-up in a resonator this is the relevant case. After enough radiation buildup, the optical field begins to bunch electrons in phase ζ_j so that the limit $E_{\rm tot}\propto N_e$ is approached. In what follows, only the emission from a single electron is calculated and the result is considered characteristic of the incoherent emission from the whole beam.

IV. RADIATION SPECTRUM

The Fourier spectrum of the Liénard-Wiechert fields can be used to solve for the infinitesimal amount of electromagnetic energy d^2E emitted into the solid angle $d\Omega$ within the frequency range $(\omega,\omega+d\omega)$ (Ref. 16):

$$\frac{d^2E}{d\Omega\,d\omega}=\frac{e^2\omega^2}{4\pi^2c}\left|\int_{-\infty}^{+\infty}dt\{\hat{n}\times[\hat{n}\times\vec{\beta}(t)]\}\exp\{i\omega[t-\hat{n}\cdot\vec{r}(t)/c]\}\right|^2\ . \tag{4.1}$$

Since an electron only accelerates inside the undulator, the limits of the time integration are $t=0$ to $L(\eta)/\beta_0c$ ($\tau=0$ to 1). For long helical undulators the emission spectrum does not depend on the azimuthal angle φ, so that we take $\varphi=0$ in $\hat{n}$. The initial position $\vec{r}(0)$ introduces a phase factor that does not affect the emission spectrum. Inserting $\vec{\beta}(\tau)$ from (1.5) and $\vec{r}(\tau)$ from (1.7) we obtain

$$\left.\frac{d^2E}{d\Omega\,d\omega}\right|_{\varphi=0}=\frac{e^2\omega^2L^2(\eta)}{4\pi^2c^3\beta_0^2}\left|\int_0^1d\tau\left[\hat{x}\left[\frac{K}{\gamma}\cos^2\vartheta\cos\Psi(\tau)+\beta_0\sin\vartheta\cos\vartheta\right]+\hat{y}\left[\frac{K}{\gamma}\sin\Psi(\tau)\right]\right.\right.$$
$$\left.+\hat{z}\left[-\beta_0\sin^2\vartheta-\frac{K}{\gamma}\sin\vartheta\cos\vartheta\cos\Psi(\tau)\right]\right]$$
$$\times\exp\left\{\frac{i\omega L(\eta)}{\beta_0c}\left[(1-\beta_0\cos\vartheta)\tau+\frac{K\sin\vartheta}{\gamma k_0L(\eta)}\left[\frac{\sin\Psi(\tau)}{(1+\eta\tau)}\right]\right]\right\}\Bigg|^2\ , \tag{4.2}$$

where $\Psi(\tau)$ is defined below (1.7). The analytical integration is carried out in the appendix but the result is not transparent. Instead we numerically obtain graphs of the spectral properties. Expression (4.2) reduces to the sum of the squares of six real integral that can be more efficiently evaluated numerically than the result (A3).

The spectrum's fundamental line shape in the forward direction is presented for a wide range of values of η in Sec. IV A. Then, in Sec. IV B, the angular features of the spectrum are examined in detail at a few selected values of η. The values for the physical parameters are $\lambda_0=3.2$ cm, $K=0.747$, $\gamma=80$, and the number of undulator periods is $N=50$.

A. Forward spectrum in the fundamental

In Fig. 2 the forward emission spectrum of (4.2) is shown for the fundamental at selected values of η between 0.0 and 0.48. The figure shows that the line becomes broader and more structured as η increases,

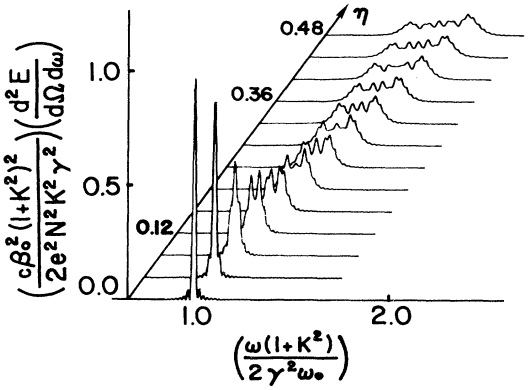

FIG. 2. Forward spectrum from a tapered undulator is shown with $0\le\eta\le0.48$, $f=1$, and $\vartheta=0$. Energy emitted is plotted in units of the forward power emission energy from an untapered undulator using the same electron energy and having the same physical parameters N, K, and λ_0.

while the center moves towards higher frequencies. These features can be understood if we think of a tapered undulator as a succession of untapered undulators whose wave number increases over the same length so that the convolution of their spectra gives a shifted line center at $\omega_0(1+\eta/2)/(1-\beta_0)$ for $\vartheta=0$.

For the tapered undulator the total spectral width can be approximated by the sum of the untapered linewidth $\sim\omega_0/N(1-\beta_0)$ and the shift in the line center caused by tapering, which is $\sim\omega_0\eta/2(1-\beta_0)$. The resulting linewidth for tapered undulators is therefore

$$\sim\omega_0(1+N\eta/2)/N(1-\beta_0) \ .$$

This estimate gives the range of frequencies over which the emitted energy drops to $\sim 5\%$ of the peak value. In Fig. 2 we show forward spectra for a range $0\leq N\eta/2\leq 12$. Note that the linewidth increases rapidly with increasing taper because of the large number of periods. In Fig. 3 the emitted energy at the line center is plotted as a function of η. The decrease in peak emission observed between $\eta=0.0$ and $\eta=0.20$ is due to the rapid increase in the spectral width together with the slower increase in the total energy radiated.

B. Angular dependence (including higher harmonics)

The angular dependence of the radiation from a tapered undulator shows the same characteristic behavior as for the untapered undulator.[6,7] Figure 4 shows the radiated energy as a function of frequency and angle in the fundamental and first three higher harmonics for the taper $\eta=0.05$. Note that the peak emission in each harmonic shifts down in frequency as the observation angle away from the undulator axis ϑ increases; the line shape remains substantially unchanged as the detector is moved off axis. The same physical arguments as presented in Sec. IV A show that the peak emission falls on a locus of points in the (ω,ϑ) plane described by

$$\omega_f=\frac{f\omega_0(1+\eta/2)}{(1-\beta_0\cos\vartheta)} \tag{4.3}$$

and the linewidth in each harmonic is given by

$$\delta\omega_f\approx\frac{\omega_0[1+(Nf\eta/2)]}{N(1-\beta_0\cos\vartheta)} \ , \tag{4.4}$$

where $f=1,2,3,\ldots$ is the harmonic number ($f=1$ is the fundamental).

An interesting aspect of (4.4) is that the linewidth depends on η and f only through their product. Therefore the spectrum in higher harmonics should have the same characteristic width as the one at lower harmonics with a higher amount of taper. Likewise reducing the tapering gives a line shape resembling the spectrum in lower harmonics. In Fig. 5 we show the shape of various spectral lines, all calculated at the fixed characteristic emission angle $\vartheta=\gamma^{-1}$. They are arranged in a square "matrix" whose rows correspond to various taperings ($\eta=0.05,0.10,0.15,0.20$) and whose columns correspond to the fundamental and the first three higher harmonics ($f=1$, 2, 3, and 4). The emission energy and frequency scales are the same for all graphs to allow for direct comparison. Notice that the matrix is nearly symmetric about the diagonal in that the line shapes corresponding to the same value of $f\eta$ are similar.

As in the case of a circularly polarized untapered undulator,[6,7] the tapered undulator generates no forward radiation in higher harmonics. In Fig. 6 we follow the radiated energy measured at the line

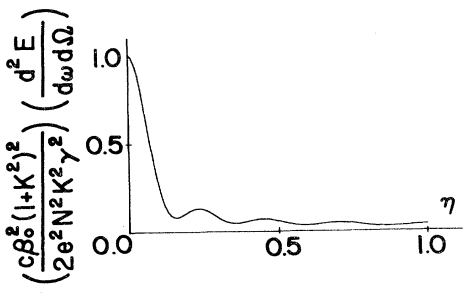

FIG. 3. Forward emission of the fundamental at the line center is plotted against the amount of taper η for $0\leq\eta\leq 1$.

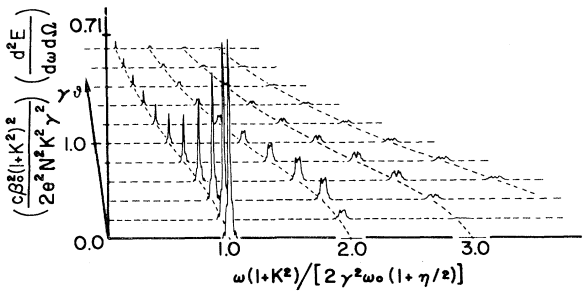

FIG. 4. Fundamental and first three higher harmonics of the emission spectrum from a tapered undulator with $\eta=0.05$ are shown as a function of frequency ω and angle in units $\gamma\vartheta$.

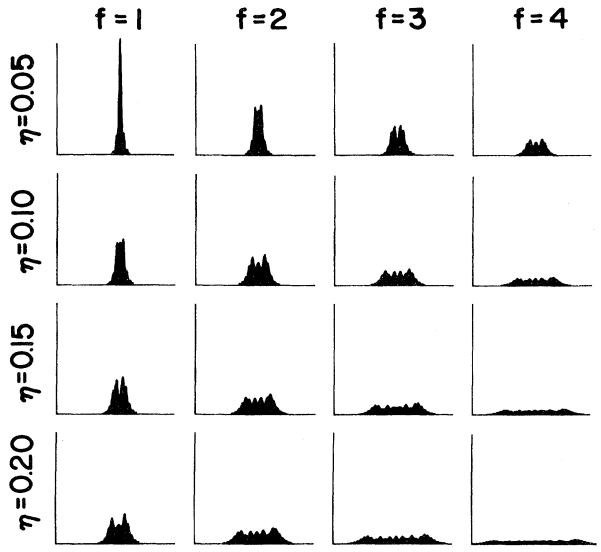

FIG. 5. Spectral line shapes $d^2E(\omega)/d\omega\, d\Omega$ are shown for $\eta=0.05$, 0.10, 0.15, and 0.20 and $f=1$, 2, 3, and 4. Line shapes corresponding to the same value of $f\eta$ are seen to be similar.

center ω_f given in (4.3) as a function of ϑ for various harmonics and tapers. Each separate graph refers to the same harmonic number, $f=1$, 2, 3, and 4, and shows the angular dependence of the peak emission for different values of taper η. At each angle the peak energy radiated into the frequency interval around ω_f decreases monotonically as η increases owing to the line broadening in (4.4).

For comparison in Fig. 7 we plot the same quantity in a linearly polarized undulator using the same physical parameters. There is now emission in the forward direction of each odd upper harmonic, $f=3,5,7,\ldots$, owing to the longitudinal acceleration of the electrons.[6,7]

V. POLARIZATION OF THE SPONTANEOUS EMISSION

The polarization of the spontaneous radiation can be studied directly by using the Liénard-Wiechert fields (3.2). From (3.2) the ratio $|E_x|^2/|E_y|^2$ is seen to be unity at $\vartheta=0$ and to vanish at the particular angle ϑ^* defined by

$$\gamma\vartheta^*=\cos^{-1}(\beta_0)\approx\sqrt{2}(1-\beta_0)^{1/2}$$
$$=(1+K^2)^{1/2} \tag{5.1}$$

for any value of taper η. For a typical value of $K=0.7$, $\gamma\vartheta^*=1.248$. As ϑ increases from 0 to ϑ^* the radiation changes polarization from circular to linear independent of the amount of tapering.

The polarization of the spontaneous radiation calculated using (4.1) can be found by projecting the integrand onto a unit polarization vector:

$$\hat{\epsilon}=(\cos\vartheta\cos\Phi,\ \cos\vartheta\sin\Phi,\ -\sin\vartheta)\ . \tag{5.2}$$

The observation angle away from the undulator axis is ϑ and the polarization angle is Φ. The spectrum shown in Fig. 8 plots the radiated energy

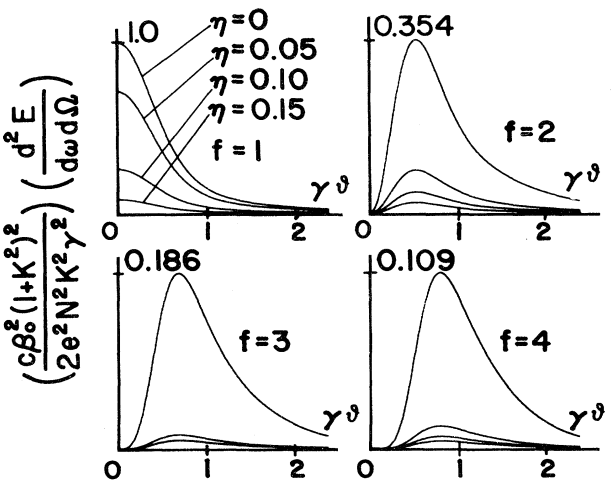

FIG. 6. Radiated energy measured at the line center frequency ω_f for the harmonics $f=1$, 2, 3, and 4 is plotted against $\gamma\vartheta$ for taperings $\eta=0.0$, 0.05, 0.10, and 0.15 for the case of a circularly polarized undulator.

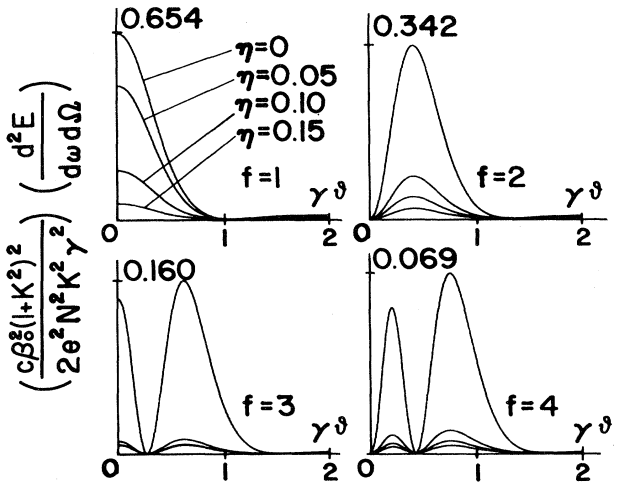

FIG. 7. Radiated energy measured at the line center frequency ω_f for the harmonics $f=1$, 2, 3, and 4 is plotted against $\gamma\vartheta$ for taperings $\eta=0.0$, 0.05, 0.10, 0.15 for the case of a linearly polarized undulator.

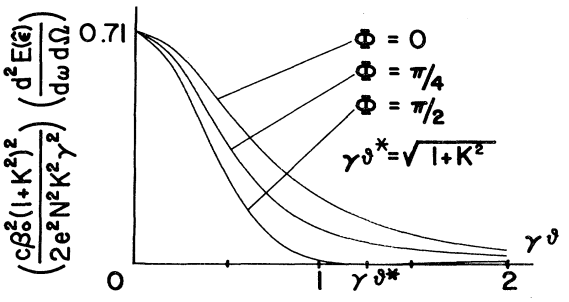

FIG. 8. Energy radiated $d^2E(\hat{\epsilon})/d\omega\, d\Omega$ with polarization $\hat{\epsilon}$ by a tapered undulator with $\eta=0.05$ is shown as a function of $\gamma\vartheta$ at the line center in the fundamental. The radiation changes its polarization from circular to linear at the angle $\gamma\vartheta^*=(1+K^2)^{1/2}$.

$d^2E(\hat{\epsilon})/d\omega\, d\Omega$ from a tapered undulator with $\nu=0.05$ as a function of ϑ measured at the line center of the fundamental for three different polarization angles $\Phi=0$, $\pi/4$, and $\pi/2$. The radiation off axis becomes progressively more polarized in the y direction and at ϑ^* the emission becomes linearly polarized as described by (5.1).

CONCLUSION

The results presented in this paper provide the first complete description of the spontaneous emission spectrum from a tapered undulator. The frequency and angular spectrum are presented for a wide range of taperings. The assumed linear dependence of $k_0(z)$ and $K=$const simplify the calculations but show the same general features expected of a wide range of tapered undulators. Practical designs are likely to be more complex in order to optimize the electron beam energy extraction during high-power laser operation. The differences will show in the detailed shapes of the spectral lines while the angular distribution and the total energy emitted will remain comparable. These results should be useful to experimentalists working on tapered FEL designs.

ACKNOWLEDGMENTS

We thank K. Speer, R. Freedman, and G. Dattoli for helpful conversations. We are grateful for research support by National Aeronautics and Space Administration Grant No. NAG-2-48 and U. S. Air Force Office of Scientific Research Grant No. AFOSR-81-0061.

APPENDIX

To perform the τ integral in (4.2) we need to rewrite the integrand. Consider the second term in the exponential of (4.2) and expand in plane waves with Bessel function coefficients[14] to write

$$\exp\left[\frac{i\omega K\sin\vartheta}{\beta_0\omega_0\gamma}\left[\frac{\sin\Psi(\tau)}{1+\eta\tau}\right]\right]$$

$$=\sum_{n=-\infty}^{\infty}J_n\left[\frac{\mu(\omega,\vartheta)}{1+\eta\tau}\right]\exp[in\Psi(\tau)]\ , \quad \text{(A1)}$$

where $\mu=\omega K\sin\vartheta/\beta_0\omega_0\gamma$. The right-hand side of (A1) can be rewritten as follows[14]:

$$\sum_{n=-\infty}^{\infty}\frac{\exp[in\Psi(\tau)]}{(1+\eta\tau)^n}\sum_{k=0}^{\infty}\frac{1}{2^k k!}J_{n+k}(\mu)\mu^k \times\left[1-\frac{1}{(1+\eta\tau)^2}\right]^k . \quad \text{(A2)}$$

If $\vartheta=0$ only the $k=0$ term survives, the double series reduces to unity, and the spectrum can then be expressed in terms of Fresnel integrals. If $\vartheta>0$ the τ integrals in (4.2) can be expressed in the general form

$$\sum_{n=-\infty}^{\infty}\sum_{k=0}^{\infty}\frac{J_{n+k}(\mu)\mu^k}{2^{k+1}k!}\int_0^1 d\tau(e^{i\Psi(\tau)}\pm e^{-i\Psi(\tau)}) \times e^{in\Psi(\tau)}e^{iw(\omega,\vartheta)\tau}\frac{(\eta\tau)^k(2+\eta\tau)^k}{(1+\eta\tau)^{n+2k}}\ , \quad \text{(A3)}$$

where

$$w=\omega L(\eta)(1-\beta_0\cos\vartheta)/\beta_0 c\ .$$

When the tapering parameter $\eta\ll 1$ (as is typically the case) an expansion in η will have terms of the form

$$\int_0^1 d\tau\,\tau^k\exp\{i[(n\pm 1)\Psi(\tau)+w(\omega,\vartheta)\tau]\}\ . \quad \text{(A4)}$$

Since $\Psi(\tau)$ is quadratic in τ, all resulting integrals can be performed analytically[14] and only the first few terms in the power-series expansion need be retained.

[1]G. A. Schott, *Electromagnetic Radiation* (Cambridge University Press, London, 1912).
[2]J. Schwinger, Phys. Rev. 75, 1912 (1949).
[3]H. Motz. J. Appl. Phys. 22, 527 (1951).
[4]D. F. Alferov, Yu. A. Bashmakov, and E. G. Bessonov, Zh. Tekh. Fiz. 43, 2126 (1973) [Sov. Phys.—Tech. Phys. 18, 1336 (1974)].
[5]B. Kincaid, J. Appl. Phys. 48, 2684 (1977).
[6]W. B. Colson, Ph.D. Dissertation (Stanford University, 1977) (unpublished).
[7]W. B. Colson, Phys. Lett. 59A, 187 (1976).
[8]J. M. J. Madey, J. Appl. Phys. 42, 1906 (1971).
[9]D. A. G. Deacon, L. R. Elias, J. M. J. Madey, G. J. Ramian, H. A. Schwettmann, and T. I. Smith, Phys. Rev. Lett. 38, 892 (1977).
[10]J. M. J. Madey, U. S. Patent No. 3,822,410 (1974).
[11]N. M. Kroll, P. L. Morton, and M. N. Rosenbluth, Phys. Quantum Electron. 7, 89 (1980).
[12]P. Sprangle, C.-M. Tang, and W. B. Manheimer, Phys. Rev. Lett. 43, 1932 (1979).
[13]C. C. Shih and M. Z. Caponi, Phys. Rev. A 26, 438 (1982).
[14]M. Abramowitz and I. A. Stegun, *Handbook of Mathematical Functions* (Dover, New York, 1964).
[15]P. Diament, Phys. Rev. A 23, 2537 (1981).
[16]J. D. Jackson, *Classical Electrodynamics* (Wiley, New York, 1975), Chap. 14.